Title: Crystallization behavior of liquid CaO-SiO_2-FeO-MnO slag in relation to its reaction with moisture

Authors: JUNCHENG LI, DEBASHISH BHATTACHARJEE, XIAOJUN HU, DIANWEI ZHANG, SEETHARAMAN SRIDHAR and ZUSHU LI

Mailing address: WMG, University of Warwick, Coventry, CV4 7AL UK

Corresponding author: ZUSHU LI

Contact e-mail: z.li.19@warwick.ac.uk

JUNCHENG LI, formerly Research Fellow with WMG, the University of Warwick, Coventry, CV4 7AL UK, is now Professor with School of Material Science and Engineering, Jiangsu University, Zhenjiang, Jiangsu Province, 212013 P. R. China. DEBASHISH BHATTACHARJEE, Global R&D Director, is with Tata Steel Research & Development, Moorgate, Rotherham, South Yorkshire, S60 3AR UK. XIAOJUN HU, Professor, is with the State Key Laboratory of Advanced Metallurgy, University of Science and Technology Beijing, Beijing 100083, P. R. China. DIANWEI ZHANG, Principal Researcher, is with Shougang Research Institute of Technology (Technical Centre), Shijingshan District, Beijing 100043. P. R. China. SEETHARAMAN SRIDHAR, formerly Tata Steel/RAEng Chair in Low Carbon Materials Technology with WMG, the University of Warwick, is now Professor with Department for Metallurgical and Materials Engineering, Colorado School of Mines, Golden, CO 80401, USA. ZUSHU LI, EPSRC Fellow in Manufacturing, is with WMG, the University of Warwick, Coventry, CV4 7AL UK. Contact e-mail: z.li.19@warwick.ac.uk.

ABSTRACT:

To help maintain the sustainability of the steel industry, we are developing a novel process to recover thermal energy (in the form of hydrogen) and valuable metal elements contained in steelmaking slags by reacting molten slags with moisture. The process is dependent on the structure and properties of the slag, of which the crystallization tendency is key, since surface phases affect the slag reactivity with the gas and enable selective formation of solid phases containing transition metals. In this paper, the precipitated phases of the molten synthetic CaO-SiO_2-FeO-MnO slags after reacting with moisture were calculated by using thermodynamic package FactSage 7.0. Laboratory experiments were conducted to reveal the crystallization behavior of the targeted metal oxides in the slags with the aim of crystallization control. A hot stage-equipped confocal laser scanning microscope (CLSM) was used to *in-situ* observe the crystal precipitation on the surface of the liquid slag after reacting with moisture. Time temperature transformation (TTT) and continuous cooling transformation (CCT) diagrams were created from the precipitation behavior of crystals during cooling in the temperature range of 1873 K to 1173 K (1600 °C to 900 °C). The microstructures of the reacted slags were analyzed with a scanning electron microscope (SEM) equipped with an energy-dispersive spectrometer (EDS) and the phases present in the slag were characterized by X-ray diffraction (XRD). TTT curves of the reacted slags (with moisture) indicated that the nose temperature and critical time for nucleation located at 1473 K (1200 °C) and 89 seconds for the slag with basicity of 1.00. Further increasing the slag basicity to 1.25 and 1.50

increased the nose temperature to 1523 K (1250 °C) and 1698 K (1425 °C) respectively. CCT curves of the reacted slags (with moisture) indicated that the crystallization temperatures of precipitated phases increased with decreasing the cooling rate from 800 K/min to 10 K/min, and the crystallization temperatures of primary phases increased with increasing slag basicity. Both magnetite (Fe_3O_4) and monoxide ($(FeO)_x(MnO)_{1-x}$) phases were detected by SEM-EDS and XRD in the reacted slags (with moisture). The amount of magnetite in the reacted slags increased from 25% to 32% to 36% and that of monoxide decreased from 5% to 2% to 1% with the slag basicity increasing from 1.00 to 1.25 to 1.50.

KEY WORDS: Crystallization; cooling rate; synthetic slag; moist gas; magnetite

I. INTRODUCTION

Steelmaking slag is one of the main by-products from the iron and steel making process. Generally, the basic oxygen steelmaking process (BOS process) generates 100 (up to 150) kg slag per ton liquid steel and ~114 Mt waste slag was generated via the BOS process worldwide in 2013. Steelmaking slags usually contain essential quantity of target metals in oxidized form during production of special and alloyed steel grades: e.g. up to 30% FeO, 3-8% MnO, 4-6% V_2O_5 and 2-9% Cr_2O_3.[1,2] The slags are produced at temperatures around 1600 ^oC and contain significant thermal energy. Up to date, the mainstream technique for the steelmaking slag treatment is known as a material for road base course material in road construction and other civil engineering projects,[3] calcium oxide-based reformer (for ground and soil

improvement),[4] raw materials for cement,[5] and fertilizer because of its excellent mechanical properties and functions.[6] However, the technical and environmental obstacles for some steelmaking slags in the above applications, such as volumetric expansion,[7] disintegration[8] and leaching of metals,[9] result in the insufficient recycling rate of steelmaking slags. Besides, the nonmagnetic metal oxides in steelmaking slags in the conventional applications from the slag are not recovered.

Targeting the recovery of metal oxides from steelmaking slags, several metallurgical processes have been developed to recycle iron from the slags, such as directly reducing FeO in steelmaking slag by graphite and coal chars,[10] smelting reduction of FeO in steelmaking slag by solid carbon.[11] However, the effective implementation of this process is constrained by unavoidable carbon footprint and large energy consumption. An alternative approach involving oxidation of divalent iron (FeO) to trivalent state (Fe_3O_4) in the liquid slags by air and subsequently separating magnetite from the quenched slag by magnetic separation has been proposed by Semykina et al.[12-14] This promising method may enable efficient selective recovery of transitional metal oxide from steelmaking slags, especially for the $CaO\text{-}SiO_2\text{-}FeO(\text{-}MnO\text{-}V_2O_3)$ bearing steelmaking slag. On the other hand, Bhattacharjee et al.[15] and Mukherjee and Bhattacharjee[16] invented a method for producing hydrogen-rich gas without generating extra CO_2 emissions by using the thermal energy of molten slag from steelmaking. FactSage calculation and laboratory study on the slag-steam reactions were also reported by Matsuura and Tsukihashi [17] and Sato et al.[18]

In our previous work, [19] preliminary studies on developing a novel process to recover energy (in the form of H_2 gas) and materials (in the form of magnetite Fe_3O_4) from steelmaking slags were reported. Based on the reaction between molten slags and moisture ($3FeO\ (l) + H_2O\ (g) = Fe_3O_4\ (s) + H_2\ (g)$), the slag crystallization behaviors not only play an important role in generating the magnetic Fe_3O_4 (spinel) phase, but can also affect the amount of H_2 generated during the slag crystallization (in contact with moisture). The generation behavior of H_2 for thermal energy recovery has been discussed in details in another paper [20], and the present work aims at investigating the crystallization behavior of synthetic molten $CaO\text{-}SiO_2\text{-}FeO\text{-}MnO$ slags after reacting with moisture. The effect of cooling rate on the detailed crystallization properties, morphologies and crystal phases were determined.

II. EXPERIMENTAL

A. *Materials and Sample Preparation*

Table 1 presents the chemical composition of designed slags and pre-melted slags analyzed by X-ray fluorescence apparatus (XRF-1800X from Shimadzu Corporation). It should be pointed out that the weight percentage of Fe^{2+} and Fe^{3+} in the pre-melted slags was ascertained by chemical titration [21] and the results indicated that the Fe^{2+} accounted for more than 95% of the total iron in all the pre-melted slags. As a result, the iron oxide in the pre-melted slags were presented in the form of FeO. All the slags were made from chemical reagents with a purity of 99.9 wt.%, supplied by Sigma Aldrich. Prior to mixing, the chemical reagents of CaO and SiO_2 were dried at 1273 K

106 (1000 °C) for 4 hours under Ar atmosphere to remove the small amount of volatiles
107 and hydrones. The dry chemical reagent powders were well mixed with FeO and
108 MnO powders based on Table 1, then put into a platinum crucible, and heated in a
109 tube furnace at 1873 K (1600 °C) for 2 hours under high purity of Ar atmosphere. The
110 temperature of the tube furnace was controlled by a program controller with an R type
111 thermocouple, within the observed precision range of ±3 K. The premelted slags were
112 then rapidly cooled to room temperature and analyzed by XRF to confirm the
113 composition. As shown in Table 1, the measured composition was generally in
114 agreement with the designed composition within the relative difference of 5%.

115 **B. *Experimental Apparatus and Procedure***

116 In this study, the crystallization event was observed optically *in situ* under the
117 CLSM (SVF-SP; Yonekura MFG. Co. LTD, Japan), and recorded at various
118 temperatures in an Ar atmosphere. The experimental assembly mainly consisted of a
119 moisture generator and the CLSM, which has been described in detail in a previous
120 publication. [19]

121 Prior to each experiment, 0.2 g of the master slag (pre-melted slag) was put into a
122 Pt crucible and then heated at the hot stage of CLSM under Ar atmosphere. To ensure
123 the slag fully melted, the sample was kept at 1873 K (1600 °C) under argon gas for 5
124 minutes and then the argon gas was switched to H_2O-Ar gas (with the H_2O partial
125 pressure of approximately 0.2 atm) to react with molten slag for 10 minutes at 1873 K
126 (1600 °C). After the reaction, the H_2O-Ar gas was switched to Ar gas and the slag was
127 quenched with three different cooling processes as shown in **Figure 1**, namely the

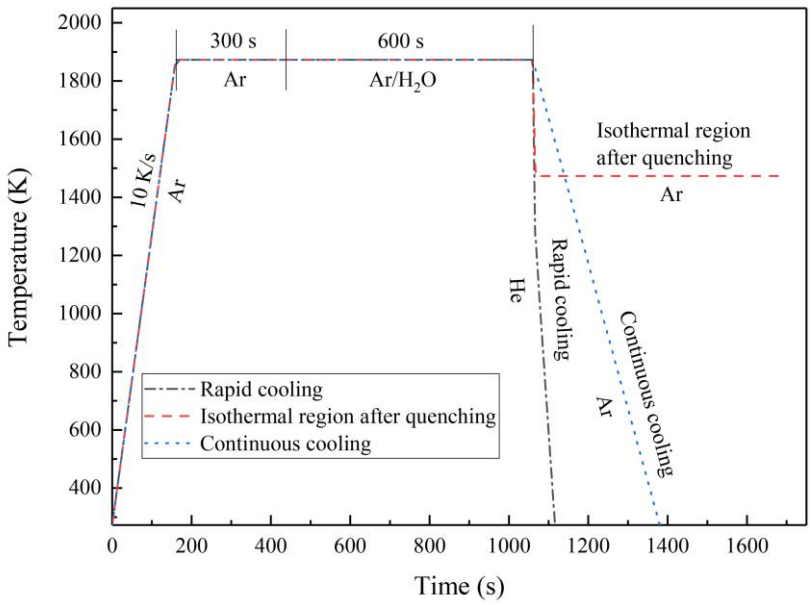

Fig.1 Thermal control of three different cooling processes

rapid cooling, the isothermal region after quenching and the continuous cooling. In the rapid cooling experiment, the fixed cooling rates of 100 K/S and 20 K/S were applied to the molten slag samples in the temperature range of 1873 K - 1273 K (1600 °C -1000 °C) and 1273 K - 323 K (1000 °C - 50 °C) respectively with the aim of obtaining amorphous slags to analyze the slag structure by using Raman Spectrometry. In the isothermal region after quenching experiment, the molten slag samples were quenched with a cooling rate of 50 K/S to a preset temperature and was held for 5-30 minutes to construct the TTT (Time Temperature Transformation) diagrams. As for the continuous cooling, a fixed cooling rate (between 10 K/min and 800 K/min) was applied to the molten slag samples being at 1873 K (1600 °C) till the end of the slag solidification to plot the CCT (Continuous Cooling Transformation) diagrams. The microstructure and mineral composition of the quenched slags were analyzed by electron scanning microscopy (Sigma from Zeiss) equipped with energy-dispersive X-ray spectroscopy (Xmax50 from Oxford Instrument) and XRD

144 (Empyrean from Panalytical) respectively.

145 Comparison experiments were carried out in parallel throughout under Ar
146 atmosphere, that is, the molten slag was held under Ar gas (instead of reacting with
147 H_2O-Ar gas) at 1873 K (1600 °C) for 10 minutes. All the other experimental
148 procedures are exactly similar. The sample obtained in the experiment of reacting with
149 H_2O-Ar gas is thereafter labelled as "Reacted" slag while the sample obtained in
150 comparison experiment (without reacting with H_2O-Ar gas) is "Un-reacted" slag.

151

152 **III. RESULTS AND DISCUSSION**

153 **A. *Thermodynamic simulation of precipitated phases***

154 To investigate the effect of gas atmospheres (reactive moist atmosphere versus inert
155 Ar) on the crystallization behavior of slags, FactSage 7.0 calculations were conducted
156 to predict the precipitated phases from both the un-reacted (in Ar) and reacted (with
157 moisture) slags with different basicities during cooling. The calculations comprised
158 three steps of molten slag equilibration in Ar, slag-gas (Ar or moisture) equilibrium
159 and molten slag solidification in Ar. The methodology of thermodynamic calculations
160 has been described in detail in the previous publication.[19] The calculated amount of
161 different phases present in the un-reacted slags with different basicities at different
162 temperatures are shown in **Figures 2(a)**, **3(a)** and **4(a)**, while that for the reacted slags
163 in **Figures 2(b)**, **3(b)** and **4(b)**. The olivine phase in Figures 2(a), 2(b), 3(a), 3(b), 4(a)

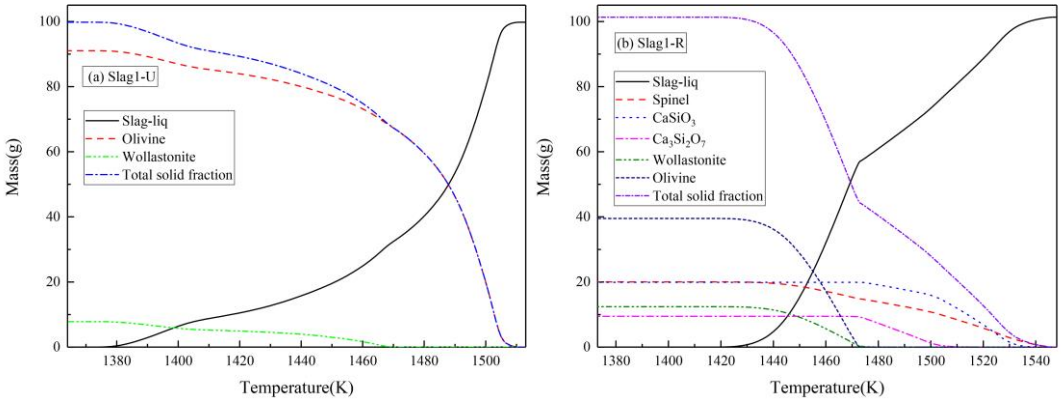

Figure 2 Change in accumulated amount of different phases precipitated from slags with basicity of 1.00 (a) un-reacted slag and (b) reacted slag

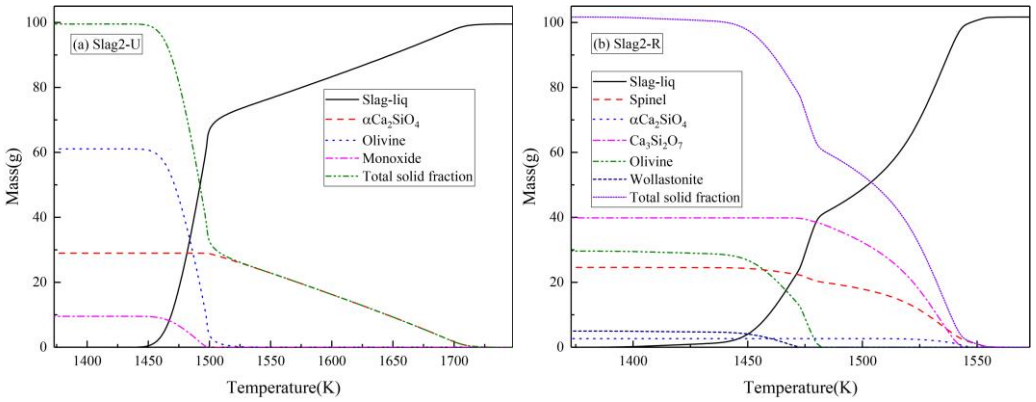

Figure 3 Change in accumulated amount of different phases precipitated from slags with basicity of 1.25 (a) un-reacted slag and (b) reacted slag

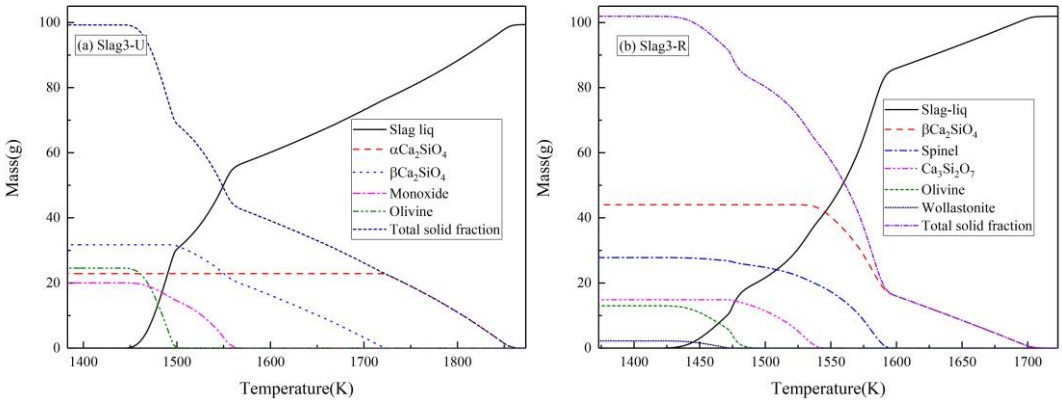

Figure 4 Change in accumulated amount of different phases precipitated from slags with basicity of 1.50 (a) un-reacted slag and (b) reacted slag

and 4(b) was the solid solution of Ca_2SiO_4-$CaFeSiO_4$-$CaMnSiO_4$, while the

174 wollastonite phase in **Figures 2(a), 2(b), 3(b)** and **4(b)** was the solid solution of
175 $CaSiO_3$-$MnSiO_3$-$FeSiO_3$. In addition, the monoxide phase in **Figure 3(a)** was the
176 solid solution of FeO-MnO-(CaO-Fe_2O_3), while the spinel phase consisted of more
177 than 60% of Fe_3O_4 and the rest of $FeMn_2O_4$. As can be seen, the temperature for the
178 precipitation of primary phase increased with increasing slag basicity from 1.00 to
179 1.25 to 1.50 for both reacted and un-reacted slags. For example, for the reacted slags
180 with basicities of 1.00, 1.25 and 1.50, precipitation of primary phase started at 1544 K
181 (1271 ℃), 1555 K (1282 ℃) and 1704 K (1431 ℃) respectively. Precipitation of
182 primary phase and disappearance of the slag liquid for the un-reacted slags with
183 basicities of 1.25 and 1.50 occurred at higher temperatures than those for the reacted
184 slags. However, for the slags with basicity of 1.00, the precipitation of primary phase
185 and disappearance of the slag liquid occurred at lower temperature for the un-reacted
186 slag than that for the reacted slags. This will be discussed in the section "C.
187 Crystallization properties of the slags under continuous cooling condition". It is
188 clearly seen that spinel phase (Fe_3O_4-$FeMn_2O_4$) was formed in the reacted slag and its
189 amount increased from 20.03 g to 24.60 g to 27.80 g (out of 100 g slag) with the slag
190 basicity increasing from 1.00 to 1.25 to 1.50. Fetters and Chipman[22] reported that the
191 activity of FeO reached a distinct local maximum corresponding to a basicity of
192 approximately 2 in the equilibria of liquid iron and CaO-MgO-FeO-SiO_2 slags.
193 Similar result was also found by Turkdogan and Pearson [23] in the liquid iron and
194 steelmaking slag system. As a result, the activity of FeO in the slags investigated in
195 this study can be considered to increase with increasing the slag basicity from 1.00 to

196 1.25 to 1.50, which facilitate the chemical reactions (1) and (2) during the molten slag
197 in contact with moisture, resulting in the increase of spinel phase (magnetite Fe_3O_4)
198 produced.

199 $$2\ FeO\ (l) + H_2O\ (g) = Fe_2O_3\ (s) + H_2\ (g) \quad (1)$$

200 $$Fe_2O_3\ (s) + FeO\ (l) = Fe_3O_4\ (s) \quad (2)$$

201 Compared with the inert Ar atmosphere, the reactive moist atmosphere enables the
202 production of spinel phase, the amount of which increases with the increasing of slag
203 basicity from 1.00 to 1.50.

204 ***B. Crystallization properties of the slags under isothermal region after quenching***

205 The crystallization evolution of the reacted slag with basicity of 1.00 under the
206 isothermal region after quenching was recorded and the images are shown in **Figure 5**,
207 where the isothermal temperature was set as 1373 K (1100 °C). Figure 5(a) and

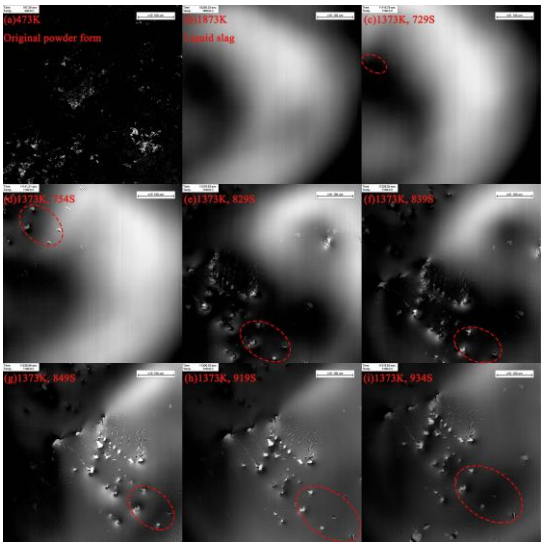

208

209 Figure 5 Crystallization process of reacted slag with basicity of 1.00 during
210 isothermal region after quenching: (a)-(b) morphology of master slag at 473 K and at
211 1873 K, respectively; (c)-(i) crystallization process of reacted slag at the temperature
212 of 1373 K for 729 S, 754 S, 829 S, 839 S, 849 S, 919 S, 934 S, respectively

Figure 5(b) showed the morphology of master slag at room temperature and at 1873 K (1600 ℃) under Ar atmosphere, respectively. As shown in Figure 5(c), a set of scaly white spots was observed at the top left corner of slag sample when the molten slag was quenched at 50 K/s from 1873 K (1600 °C) to 1373 K (1100 °C) and kept for 729 S at 1373 K (1100 °C). Thereafter, the volume and growth of the crystal nucleus increasingly extended from the edge to the center of slag sample, accompanying the shift of crystals from top left corner to bottom right corner (Figure 5(d) -5(i)).

Onsets of slag crystallization were observed under CLSM and recorded to construct the TTT (time-temperature-transformation) diagrams for the un-reacted (**Figure 6**) and reacted slags (**Figure 7**). The un-reacted slags (Figure 6) showed a

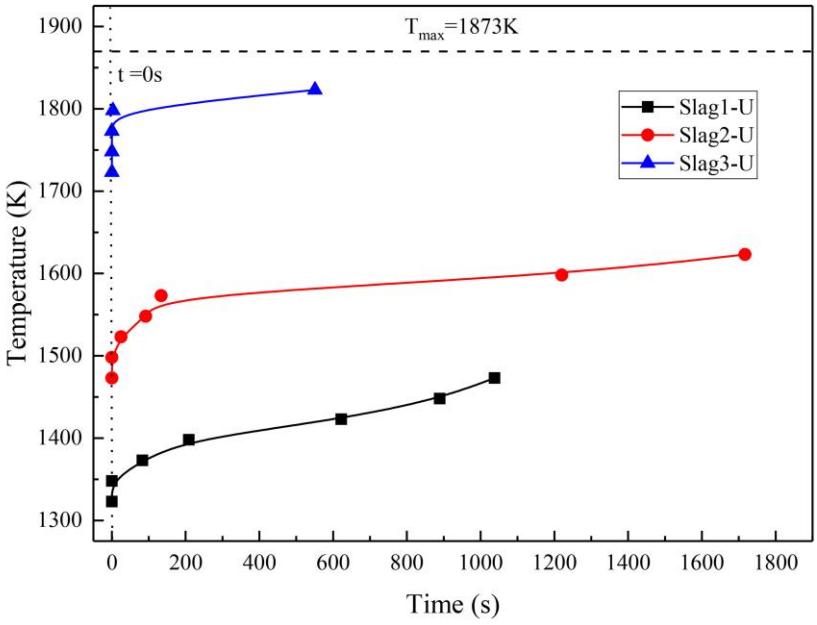

Figure 6 TTT diagram of un-reacted slags with different basicities

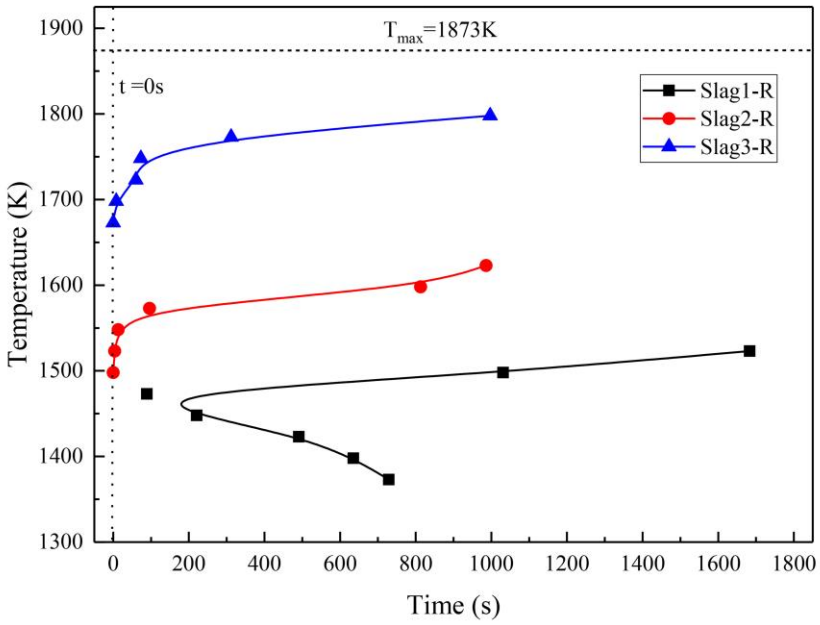

Figure 7 TTT diagram of reacted slags with different basicities

half-'C'-shaped TTT curve, and the nose temperature increased while the critical time for nucleation decreased when the slag basicity increased from 1.00 to 1.50. Compared with the TTT curve of the un-reacted slags, the reacted slag (Figure 7) with basicity of 1.00 shows a typical 'C'-shaped TTT curve, with the apparent nose of the TTT located at 1473 K (1200 °C) and 89 seconds. However, a half-'C'-shaped TTT curves were presented for the reacted slags with basicity of 1.25 and 1.50, and the nose temperature increased from 1523 K (1250 °C) to 1698 K (1425 °C) with the slag basicity increasing from 1.25 to 1.50.

As evident from Figure 7, with increasing basicity of the reacted slags, not only did the TTT curves of glassy to crystalline transformation shift to the left, but also the TTT diagrams shifted to higher temperatures, indicating higher tendency for crystallization. This is consistent with the trend observed in fluoride-free mould fluxes that the crystallization temperature increases with increasing basicity. [24]

In order to compare the crystallization behavior of the un-reacted and reacted slags

with different basicities, the critical cooling rate, i.e. the minimum cooling rate that results in a completely glassy slag (i.e. no crystalline content), can be expressed by Eq. (3) [25, 26]

$$R_{c,TTT} = \frac{T_{max} - T_{nose}}{t_{nose}} \quad (3)$$

Where, $R_{c,TTT}$ is the critical cooling rate in TTT diagram, $T_{\max}$ is the melting temperature before cooling, T_{nose} and t_{nose} are the temperature and time corresponding to the nose in TTT diagram. **Table 2** presents the calculated values of the critical cooling rates for the un-reacted and reacted slags with different basicities. For the un-reacted and reacted slags with basicity of 1.00, the critical cooling rate was 390 K/minute and 269 K/minute respectively, which suggests that cooling rates above these values will likely result in an amorphous structure. This is in agreement with the results that no crystallization occurred at the cooling rates of 400 K/min for both un-reacted and reacted slags under continuous cooling in section C of this study. For the slags with basicity of 1.25 and 1.50, the critical cooling rates were 840 K/min and 1500 K /min for the un-reacted slags, and 5250 K/min and 1313 K/min for the reacted slags with basicity of 1.25 and 1.50.

The difference of crystallization temperature predicated by thermodynamic calculation and observed by CLSM should be attributed to the difference of equilibrium condition (equilibrium cooling in thermodynamic calculation and non-equilibrium cooling in experiment) and the limited resolution of CLSM.

C. Crystallization properties of the slags under continuous cooling condition

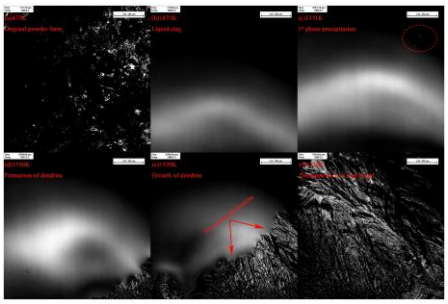

Figure 8 Crystallization process of un-reacted slag with basicity of 1.0 at the continuous cooling rate of 10 K/min: (a)-(b) morphology of master slag at 473 K and at 1873 K, respectively; (c)-(f) crystallization process of un-reacted slag at the temperature of 1331 K, 1330 K, 1329 K, 1328 K, respectively

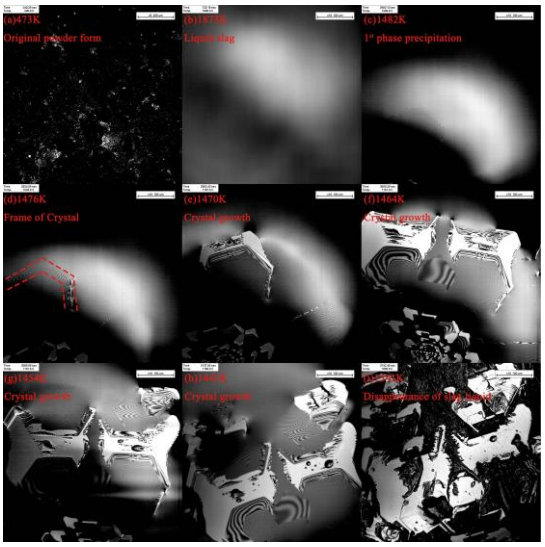

Figure 9 Crystallization process of reacted slag with basicity of 1.0 at the continuous cooling rate of 10 K/min: (a)-(b) morphology of master slag at 473 K and at 1873 K, respectively; (c)-(i) crystallization process of reacted slag at the temperature of 1482K, 1476 K, 1470 K, 1464 K, 1454 K, 1441 K, 1359 K, respectively

Figure 8 and **Figure 9** show the crystallization behavior of the un-reacted and reacted slags with basicity of 1.0 observed by CLSM at the cooling rate of 10 K/min respectively. In comparison, a non-equiaxed dendritic morphology was observed for the un-reacted slag in Figure 8(e), while a hexagonally faceted crystal was observed

for the reacted slag in Figure 9(f). There are various investigations regarding the effects of undercooling [27,28], slag composition [29,30] and enthalpy of mixing (so-called Jackson α factor)[31,32] on morphology of melt crystalline. The different morphological evolution for "Reacted" and "Un-reacted" slags could be attributed to some or all of these factors (undercooling, slag composition and enthalpy of mixing), which will be reported in a separate paper.

It is noticeable that a very small temperature region from 1330 K to 1328 K (1057 ℃ to 1055 ℃) between formation of non-equiaxed dendrite and fully crystallization of liquid slag was observed in the un-reacted slag (Figure 8(d)-8(f)). On the contrary, a large temperature region from 1476 K to 1359 K (1203 ℃ to 1086 ℃) between formation of hexagonally faceted crystal and fully crystallization of liquid slag was observed in the reacted slag with the basicity of 1.0 (Figure 9(d)-9(i)).

Figures 9(a) and 9(b) show the morphology of the master slag (pre-melted slag) at room temperature and at 1873 K (1600 ℃) under Ar atmosphere, respectively. The nucleus of the primary crystal phase were observed to form at 1482 K (1209 ℃) in Figure 9(c), and the frame of crystal formed at ~1476 K (1203 ℃) in Figure 9(d). With decreasing the temperature from 1470 K (1197 ℃) to 1441 K (1168 ℃), the volume of the crystal nucleus increased gradually (Figure 9(e)-9(h)). Finally, the liquid slag appeared to have fully crystallized at 1359 K (1086 ℃) in Figure 9(i). It should be pointed out that the crystallization temperature of a precipitated phase was assumed to be the temperature when the crystal nucleus first came into the sight under CLSM observation although the crystal nucleus might form ahead of the observation

due to the limited resolution of CLSM.

CCT diagrams of the un-reacted and reacted slags with different basicities were determined and shown in **Figure 10** and **Figure 11**. In general, the crystallization

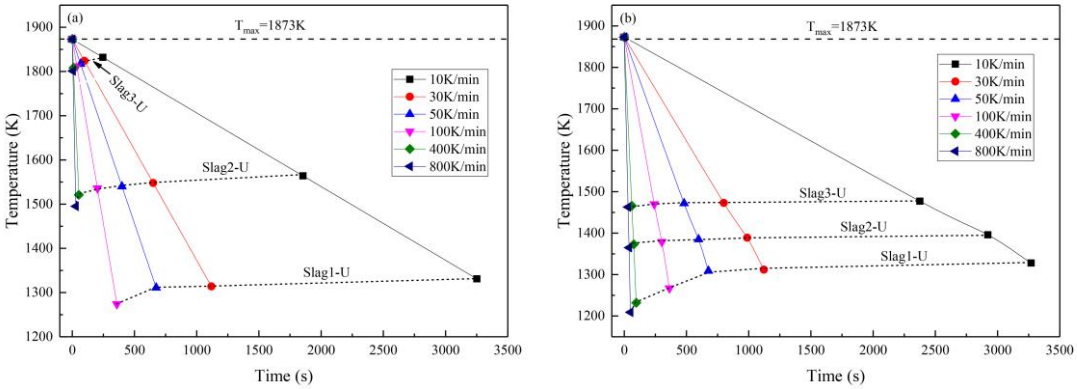

Figure 10 CCT diagram for the un-reacted slags with different basicities (a) starting crystallization of primary phase and (b) full crystallization of slag

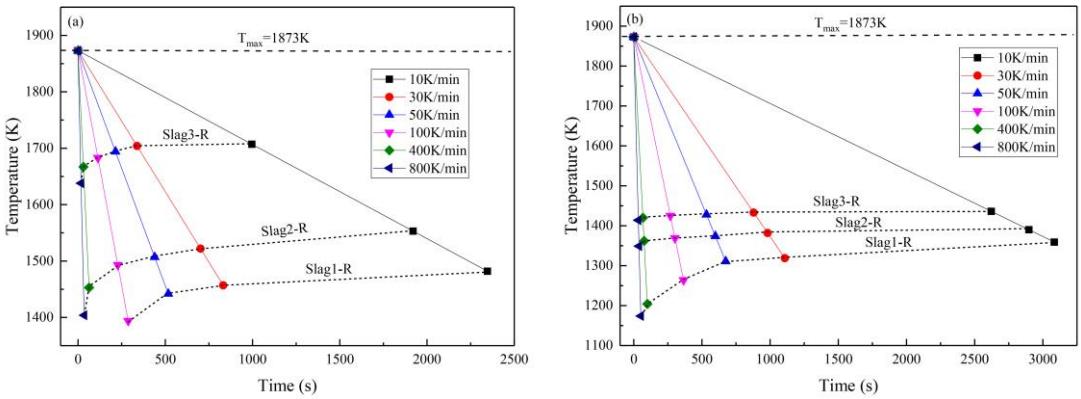

Figure 11 CCT diagram for the reacted slags with different basicities (a) starting crystallization of primary phase and (b) full crystallization of slag

temperatures of precipitated phases became lower with increasing the cooling rate from 10 K/min to 800 K/min, which is to be expected. A similar trend was reported previously concerning the crystallization behavior of synthetic coal ash slag [33] and BOF slag [34] under different cooling rates. It can be understood that the increasing of cooling rates resulted in larger increase in slag viscosity as temperature was lowered

312 before crystallization commenced enabling a higher degree of undercooling (a lower
313 crystallization temperature).[35]

314 Besides, the crystallization temperatures of primary phases increased with the
315 increasing of slag basicity. The crystallization temperature was not observed during
316 rapid cooling between 400 K/min and 800 K/min for the slag with basicity of 1.00 in
317 this study. This trend suggests that melts which are more basic have a higher tendency
318 for crystallization. This not only agrees with the fact that a great number of breakage
319 of Si-O bonds and re-ordering of silicate structure, resulting in a lower viscosity,
320 occurs with increasing basicity, but also is in accordance with the observed
321 crystallization behavior of $CaO\text{-}SiO_2\text{-}Al_2O_3\text{-}MgO$ slags with different basicities
322 investigated by Esfahani and Barati.[36]

323 For the slags with basicities of 1.25 and 1.50, precipitation of primary phase started
324 at higher temperature for un-reacted slag than that for reacted slag. For example, for
325 the slag with basicity of 1.50 and at cooling rate of 10 K/min, precipitation of primary
326 phase in un-reacted slag started at 1832 K (1559 ℃) higher than 1638 K (1365 ℃)
327 for reacted slag. However, the trend for the slag with basicity of 1.00 is reverse, that is,
328 the precipitation of primary phase in un-reacted slag started at a lower temperature
329 than that for reacted slag at the same cooling rate. This is in accordance with the
330 thermodynamic calculation results in Figure 2 to Figure 4 and may be explained by
331 the variation of viscosity in the un-reacted and reacted slags.

332 The structure of the amorphous slags (i.e. the quenched slags after reacting with
333 moisture or holding in Ar gas) was analyzed using Raman spectroscopy (Renishaw

inVia Reflex Raman, Gloucestershire, UK) with a 532 nm laser. The same experiment has been repeated for five times to obtain sufficient slag for Raman analysis. The

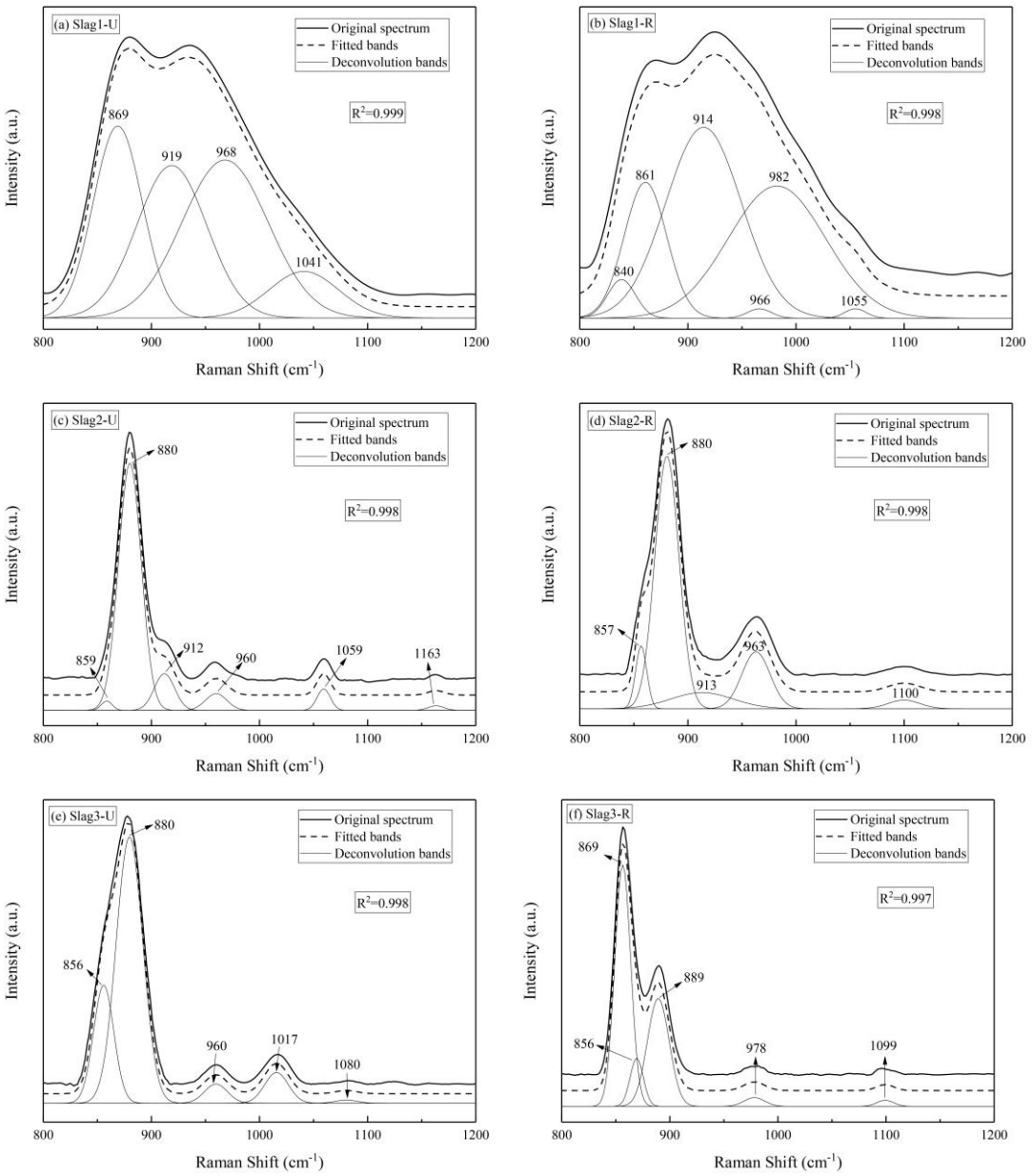

Figure 12 Deconvoluted Raman spectra of amorphous slags with different basicities: (a) Slag1-U; (b) Slag1-R; (c) Slag2-U; (d) Slag2-R; (e) Slag3-U; (f) Slag3-R

Raman spectra were concentrated between 1200 and 800 cm^{-1} and deconvoluted by Fityk 0.9.8 software, as shown in **Figure 12**. Accordingly, all the bands were assigned with the corresponding species and the relative abundance of each species

semi-quantitatively expressed in their area percentage are listed in **Table 3.** Early studies by Russel,[46] Orrling,[47] and Baek et al.[48] on the solubility of H_2O in molten slags revealed that water vapor dissolves in molten slags in form of hydroxyl ion or hydroxyl radical. However, in this study, no band was found to be the -OH stretching vibration for both the reacted and un-reacted slags. From the results shown in Figure 12 and Table 3, it is seen that the symmetric stretching vibration of several types of band groups for Si corresponding to Q^0 (monomer), Q^1 (dimer), Q^2 (Chain) and Q^3 (sheet) are observed at about 850-880 cm^{-1}, 900-920 cm^{-1}, 950-980 cm^{-1} and 1050-1120 cm^{-1}. In addition, the Si-O stretching vibration is found at the 889cm^{-1}, 1017cm^{-1} and 1041cm^{-1}, while the symmetric stretching vibration of Si-O-Si is seen at 840 cm^{-1}, 1080 cm^{-1} and 1163 cm^{-1}. The distribution of the Q species was examined and the values of $(Q^0+Q^1)/(Q^2+Q^3)$ were calculated to evaluate the depolymerization degree of the slags in **Table 4**.

As shown in Table 4, with the increasing of slag basicity from 1.0 to 1.5, the depolymerization degree, $(Q^0+Q^1)/(Q^2+Q^3)$, increase from 1.47 to 21.59 for the un-reacted slags and from 1.52 to 15.72 for the reacted slags, which is in agreement with the general belief that the basic oxide CaO, as a so-called network modifier, can depolymerize silicate network structure by the formation of non-bridging oxygen. As for the effect of gas atmosphere on the slag structure, the depolymerization degree for the un-reacted slags with basicity of 1.25 and 1.50 is higher than those for the reacted slags, while for the slags with basicity of 1.00, the depolymerization degree is lower for the un-reacted slag than that for the reacted slags. This trend agrees with the

366 thermodynamic calculation results in Figure 2 to Figure 4 and the crystallization
367 behavior observed by CSLM as shown in Figure 10 and Figure 11. Because Raman
368 spectroscopy is based upon the polarizability of the silicates, whereas IR is based
369 upon the dipole moment change, samples can be either Raman or IR active in certain
370 cases depending upon the chemical environment of the slag. Therefore FTIR analysis
371 is used in this study to complement the Raman spectroscopy and the FTIR results are
372 detailed in Appendix.

373 The difference in slag composition between the unreacted and reacted slags at same
374 slag basicity is Fe^{3+} content in the reacted slag has substantially increased because of
375 the reaction of molten slag with moisture (in the previous step before quenching)
376 compared to the unreacted slag, which can affect the depolymerization degree
377 between the reacted and un-reacted slags. The structural behavior of iron oxide (ferric
378 and ferrous) and its composition dependence has been a long standing research topic,
379 and the views from different researchers can be contrasting.[49, 50] Because of the
380 amphoteric nature of Fe^{3+}, Fe^{3+} can be both a network former (tetrahedral structure) and
381 a network breaker (octahedral coordination), which is dependent on the slag
382 composition. The amphoteric nature of Fe^{3+} can also explain well the difference in
383 depolymerization between the reacted and un-reacted slags. For the higher slag
384 basicity slag (1.25 and 1.50), ferric iron can be considered as a network former, which
385 results in the lower depolymerization degree in the reacted slag (with higher Fe^{3+})
386 than that in un-reacted slag (with lower Fe^{3+}). For the lower basicity slag (1.00), ferric
387 iron can be considered as a network-breaker causing higher depolymerization degree

in reacted slag (with higher Fe^{3+}) than that in un-reacted slag (lower Fe^{3+}), although the difference in depolymerization between the reacted and un-reacted slags for lower basicity (1.00) is very small.

It is interesting to note that, in Figures 10(a) and Figures 11(a), increasing cooling rate decreases to certain extent the crystallization temperature of primary phase but substantially reduces the crystal incubation time. For example, for the reacted slag with basicity of 1.00, temperature decreases from 1482 K to 1394 K (1209 °C to 1121 °C), while the crystal incubation time sharply reduced from 2346 S to 287 S with increasing of cooling rate from 10 K/min to 100 K/min. This indicates that the slag with the basicity of 1.00 requires a longer crystal incubation time when the cooling rate is below 100 K/min, which should be attributed to the easier formation of an amorphous structure in low basicity of 1.00 than the high basicity of 1.25 and 1.50, extending the crystal incubation time of low basicity slag.[51]

Figure 13 shows the influence of the cooling rate on undercooling degree (from

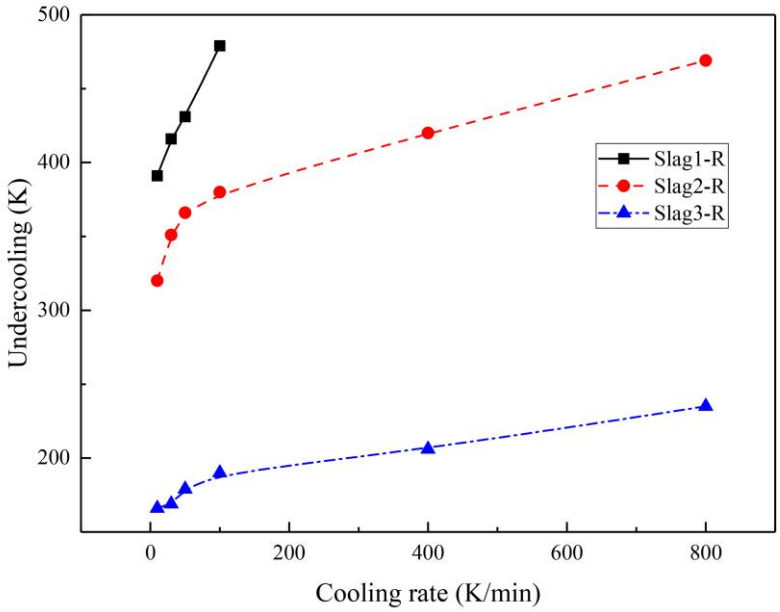

Figure 13 Influence of cooling rate on undercooling degree of reacted slags with

404 different basicities

405 melting temperature to the temperature of starting crystallization)[52] of reacted slags
406 with different basicities. The undercooling degree required for the slag crystallization
407 increased with decreasing slag basicity at all the cooling rates investigated. For
408 example, at the cooling rate of 10 K/min the undercooling degree for the reacted slag
409 increased from 166 K to 320 K to 391 K with decreasing the slag basicity from 1.50
410 to 1.25 to 1.00.

411 The crystallization behavior of the slags under isothermal region after quenching
412 (TTT curve) and continuous cooling (CCT curve) provide useful information, such as
413 temperature, crystal incubation time and critical cooling rate, for recovering the
414 targeted phase (magnetite Fe_3O_4) from synthetic CaO-SiO_2-FeO-MnO slags, which
415 help design processes for the recovery of valuable elements (Fe, Mn etc) in the slags.

416 **D. *Phase characterization***

417 **Figure 14** shows the CLSM morphology of the crystalline in the reacted slag with

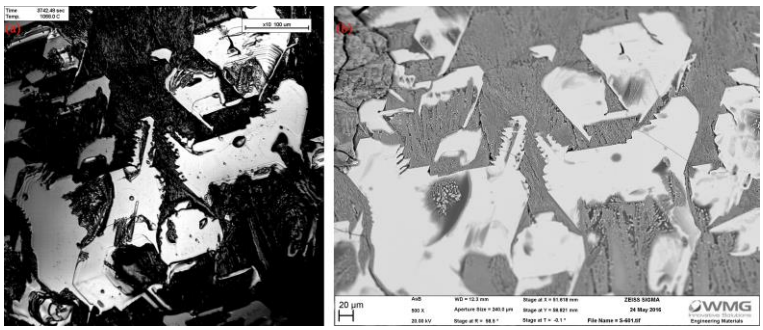

418

419 Figure 14 Morphologies of the crystalline in the reacted slag with the basicity of 1.0 at
420 continuous cooling rate of 10 K/min (a) CLSM image and (b) SEM image

421 the basicity of 1.00 at continuous cooling rate of 10 K/min and the corresponding
422 SEM morphology. It indicated that morphologies of the crystalline observed by

CLSM are in well agreement with those by SEM. As shown in **Figure 15**, mainly

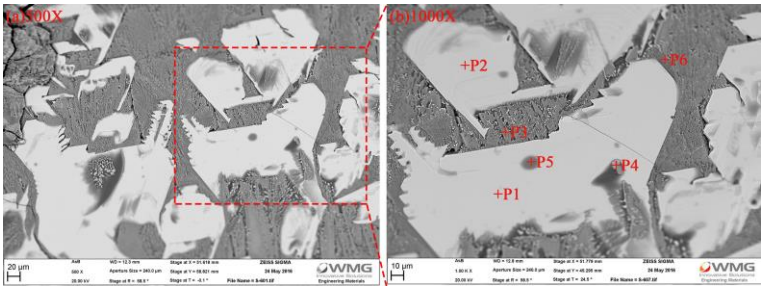

Figure 15 SEM photographs of reacted slag with the basicity of 1.0 at the continuous cooling rate of 10 K/min with different magnification factors: (a) 500X and (b) 1000X

three phases in the reacted slag were observed, namely the white equiaxed phase (P1 and P2), grey dendritic crystal (P3 and P4) and slag matrix (P5 and P6). The diameter of these white crystals was approximately 100 μm. It is noticeable that these white crystals existed locally and were surrounded by vast amounts of grey dendritic crystal, indicating an early crystallization, in comparison to slag matrix and grey dendritic crystal. In order to determine the elementary distribution in different phases, EDS mapping analysis was employed and the corresponding results were presented in Figure 16. Ca and Si were mainly enriched in the grey phase as matrix phase, while

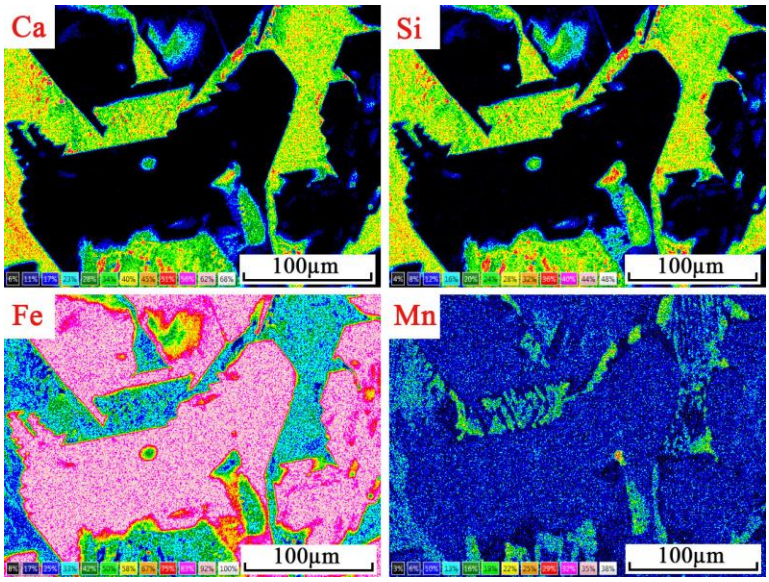

Figure 16 EDS map scanning of reacted slag with basicity of 1.0 at the continuous

cooling rate of 10 K/min

Fe was mainly concentrated in the white phase. Moreover, Mn was mainly concentrated in the grey dendritic crystal. EDS spot analysis (**Table 5**) indicated that the white phase was close to $Fe_3O_{3.8}$, while the grey dendritic crystal and slag matrix were approaching $CaMn_{1.14}Fe_{1.70}Si_{1.89}O_{6.25}$ and $CaSiFe_{0.62}O_{3.67}$ respectively.

The phases presented in the reacted slags with different basicities at the continuous cooling rate of 10 K/min were characterized by XRD and the results are shown in **Figure 17** to **Figure 19**. In general, there were mainly four different phases detected

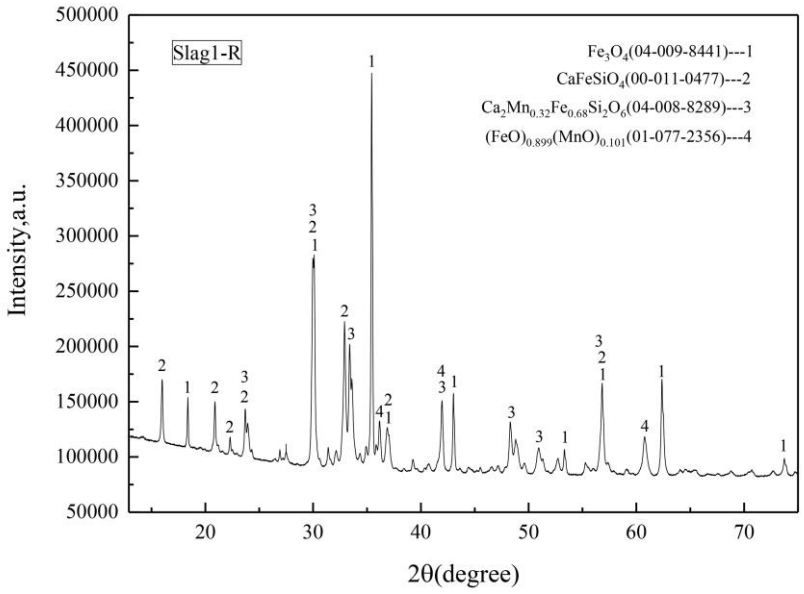

Figure 17 X-ray diffraction patterns of reacted slag with the basicity of 1.00 at the continuous cooling rate of 10 K/min

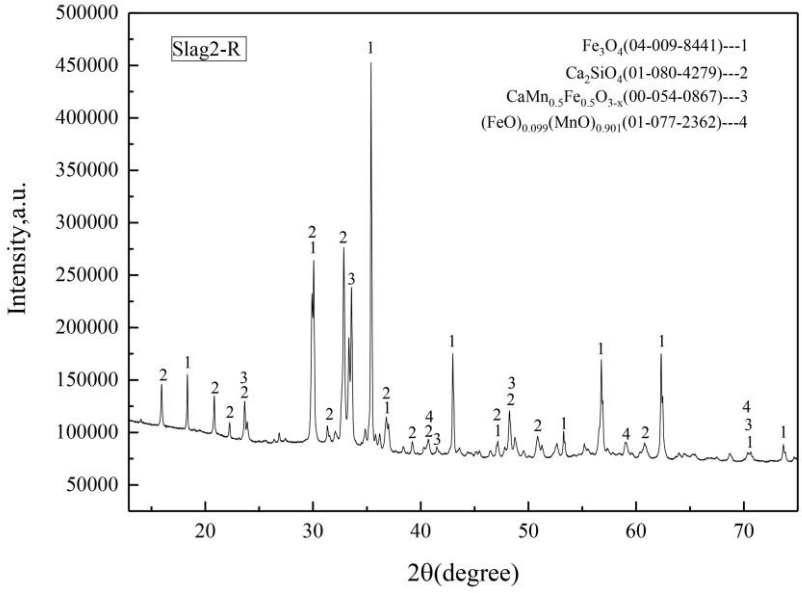

448

449 Figure 18 X-ray diffraction patterns of reacted slag with the basicity of 1.25 at the

450 continuous cooling rate of 10 K/min

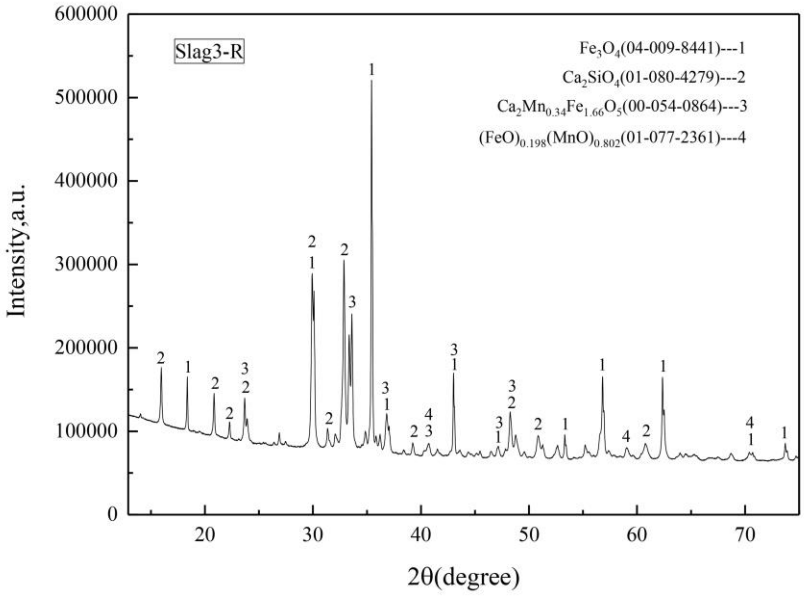

451

452 Figure 19 X-ray diffraction patterns of reacted slag with the basicity of 1.50 at the

453 continuous cooling rate of 10 K/min

454 in the reacted slags, including both magnetite (Fe_3O_4) and monoxide ($(FeO)_x(MnO)_{1-x}$)

455 phases in each slag. The appearance of Fe_3O_4 indicated the oxidization of Fe^{2+} to Fe^{3+}

456 occurred in the reaction between molten CaO-SiO_2-FeO-MnO slags and moisture gas,

while the presence of monoxide indicated the incomplete oxidization of transition metal oxides (such as Fe^{2+} and Mn^{2+}) due to various kinetic factors such as the reaction time, the reaction area of the slag-gas system. As for the reacted slag with the basicity of 1.00 (Figure 17), the main phases were detected to be spinel (magnetite Fe_3O_4), $CaFeSiO_4$ and $CaMn_{0.32}Fe_{0.68}Si_2O_6$ with a small amount of $(FeO)_{0.899}(MnO)_{0.101}$. As for the reacted slag with the basicity of 1.25, as shown in Figure 18, four phases detected were: spinel (magnetite Fe_3O_4), Ca_2SiO_4, $CaMn_{0.5}Fe_{0.5}O_{3-x}$ and $(FeO)_{0.099}(MnO)_{0.901}$. Similar to the phases in the reacted slags with the basicity of 1.0 and 1.25, four phases in the reacted slag with the basicity of 1.50 (Figure 19) were spinel (magnetite Fe_3O_4), Ca_2SiO_4, $Ca_2Mn_{0.34}Fe_{1.66}O_5$ and $(FeO)_{0.198}(MnO)_{0.802}$.

In comparison with the phases presented in the reacted slags, **Figure 20** shows the

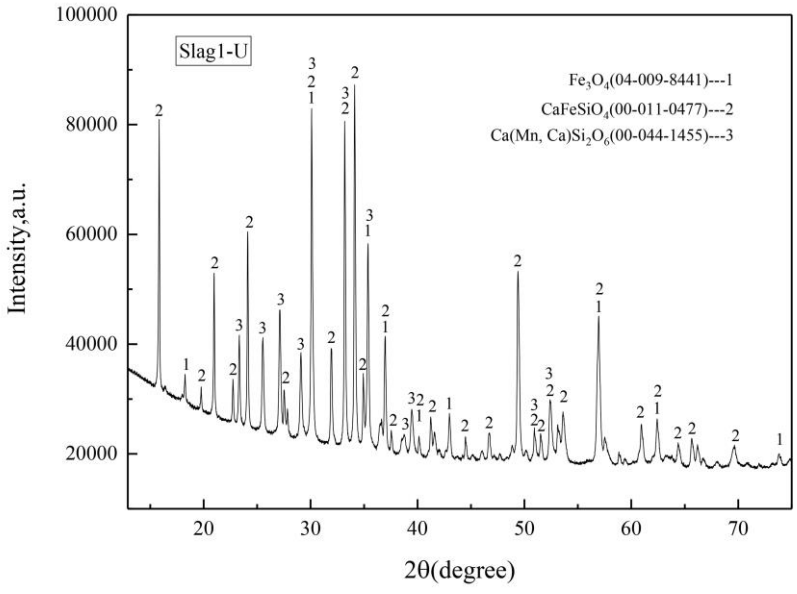

Figure 20 X-ray diffraction patterns of un-reacted slag with the basicity of 1.00 at the continuous cooling rate of 10 K/min

phases presented in the un-reacted slag with the basicity of 1.00 at the continuous cooling rate of 10 K/min. It was shown clearly that the main phases detected were $CaFeSiO_4$ and $Ca(Mn, Ca)Si_2O_6$, with a small amount of spinel (magnetite Fe_3O_4). This small amount of spinel phase (magnetite Fe_3O_4) detected in the un-reacted slag could be attributed to the oxidation of slag by the low oxygen partial pressure in highly purified Ar gas. The difference in the crystallization behavior between the un-reacted and reacted slags clearly evidenced the occurrence of the chemical reactions (1) and (2) in contact with moisture and its crystallization behavior. The differences of the precipitated phases predicted by FactSage 7.0 (Figures 2-4) with those characterized by XRD (Figures 17-20) could be attributed to the different conditions for the calculations and laboratory experiments. In this study the commercial thermodynamic package FactSage 7.0 has been used for the purpose of predicting the trends and limits of the related reactions under equilibrium state. However, in the actual crystallization process, these reactions are affected by various kinetic factors such as the reaction time, the reaction area of the slag-gas system, etc. This results in the differences of the precipitated phases predicted by FactSage 7.0 with those characterized by XRD.

By comparing the integrated intensities of the diffraction peaks from each of the known phases, the weight fraction of spinel (magnetite) phase in the un-reacted and reacted slags were semi-quantitatively determined and listed in **Table 6**. As seen in Table 6, while that in the un-reacted slag with basicity of 1.00 is 4%, the amount of magnetite in the reacted slags increased from 25% to 32% to 36% with increasing the

494 slag basicity from 1.0 to 1.25 to 1.5. Meanwhile, the amount of monoxide in the
495 reacted slags decreased from 5% to 2% to 1% with the slag basicity increasing from
496 1.0 to 1.25 to 1.5.

497 By combining the crystallization behavior observed by CLSM, the microstructure
498 analyzed by SEM-EDS and the phases present in the slags characterized by XRD, for
499 the reacted slag with basicity of 1.00, the primary phase formed at 1482 K (1209 ℃)
500 in Figure 9(c) can be considered to be Fe_3O_4. This agrees with the calculation result
501 by FactSage 7.0 (Figure 2(b)). Similarly, the primary phases formed in the reacted
502 slags with basicity of 1.25 and 1.50 should be considered as Fe_3O_4 and Ca_2SiO_4
503 respectively but were not reproduced here for the brevity of the paper.

504 The current study shows that the reaction between molten slag and the moist gas
505 atmosphere can greatly promote the conversion from FeO in the slag to magnetic
506 Fe_3O_4 (spinel) phase. This provides the possibility to recover the target iron oxides in
507 the form of magnetic spinel phase from the slag bulk via magnetic separation by using
508 the difference in magnetic susceptibility between the obtained compounds (spinel
509 phase) and slag matrix (silicate). As illustrated in Figure 15, the diameter of the spinel
510 crystals under the experimental conditions was approximately 100 μm, which not only
511 greatly simplifies the processing method, but also lowers energy consumption in
512 magnetic separation.

513 As an alternative to magnetic separation for solidified slags, a novel method to
514 separate the obtained compounds (e.g. spinel phase) from molten slags by
515 supergravity has been successfully applied in separating perovskite from

titanium-bearing slag [53], concentrating vanadium-containing spinel phase from vanadium slag [54] and enriching britholite ($Ca_3Ce_2[(Si, P)O_4]_3F$) phase from rare earth-rich slag [55]. Considering the density difference between molten slag and solid phase (Fe_3O_4 for the slag with basicity of 1.00 and Ca_2SiO_4 phase for the slag with basicity of 1.50 and above), it may be possible to separate spinel phase from molten steelmaking slag by supergravity. However, the possibility of the aforementioned two methods has not been studied so far, and further investigation should focus on how to effectively recover targeted metal oxides from the steelmaking slags after reacting with moist gas atmosphere.

IV. CONCLUSIONS

In this study, the precipitated phases of the molten synthetic CaO-SiO_2-FeO-MnO slags after reacting with moisture were firstly calculated by using thermodynamic package FactSage 7.0, and then the crystallization behavior of the slags was *in-situ* investigated by using the CLSM under the isothermal region after quenching (TTT diagram) and continuous cooling conditions (CCT diagram). The crystalline phases were characterized by using SEM-EDS and XRD. The main conclusions are obtained as follows.

Thermodynamic calculations indicated that the reactive moist atmosphere enabled the production of spinel phase, and its amount increased from 20.03 g to 24.60 g to 27.80 g (out of 100 g slag) with the slag basicity increasing from 1.00 to 1.25 to 1.50.

TTT curves of the reacted slags (with moisture) indicated the nose temperature and critical time for nucleation located at 1473 K (1200 °C) and 89 seconds for the slag

with basicity of 1.00, and the nose temperature increased from 1523 K (1250 °C) to 1698 K (1425 °C) with the slag basicity increasing from 1.25 to 1.50.

CCT curves of the reacted slags (with moisture) indicated that the crystallization temperatures of precipitated phases increased with decreasing the cooling rate from 800 K/min to 10 K/min, and the crystallization temperatures of primary phases increased with the increasing of slag basicity.

Both magnetite (Fe_3O_4) and monoxide ($(FeO)_x(MnO)_{1-x}$) phases were detected in reacted slags (with moisture). The amount of magnetite in the reacted slags increased from 25% to 32% to 36% and that of monoxide decreased from 5% to 2% to 1% with the slag basicity increasing from 1.00 to 1.25 to 1.50. The primary phase changed from magnetite (Fe_3O_4) to magnetite (Fe_3O_4) to Ca_2SiO_4 with the increasing of slag basicity from 1.00 to 1.25 to 1.50.

ACKNOWLEDGEMENT

This work was supported by Innovate UK (for Tata Steel UK), EPSRC (for University of Warwick, Grant No. EP/M507829/1), and MOST (Ministry of Science and Technology) China (for USTB and Shougang Corp.) under the project No. 102170. J LI and Z LI would like to acknowledge the support from Jiangsu University (19JDG011) and EPSRC (EP/N011368/1) separately.

560 **REFERENCES**

561 [1] A. Semykina, V. Shatokha, M. Iwase and S. Seetharaman, *Metall. Mater. Trans. B*,
562 2010, vol. 41B, pp. 1230-39.

563 [2] V. Shatokha, A. Semykina, J. Nakano, S. Sridhar and S. Seetharaman, *J. Min.*
564 *Metall. Sect. B-Metall.*, 2013, vol. 49, pp. 169 -74.

565 [3] L. S. Pioro, and I. L. Pioro, *Waste Management*, 2004, vol. 24, pp. 371- 79.

566 [4] K. Horii, T. Naoto, Y. Kitano and T. Kato, *Nippon Steel Technical Report*, 2013,
567 vol. 104, pp. 123-29.

568 [5] R. I. Iacobescua, D. Koumpouri, Y. Pontikesc, R. Sabana and G. N.
569 Angelopoulos, *J Hazard. Mater.*, 2011, vol. 196, pp. 287-94.

570 [6] M. Makelaa, G. Watkins, R. Poykio, H. Nurmesniemiet and O. Dahl, *J Hazard.*
571 *Mater*., 2012, vol. 207-208, pp. 21-27.

572 [7] L. M. Juckes, Trans. Inst. *Min. Metall. C*, 2003, vol. 112, pp. 177-97.

573 [8] F. Engström, D. Adolfsson, Q. Yang, C. Samuelsson and B. Björkman, *Steel*
574 *research int.*, 2010, vol. 81, pp. 362-71.

575 [9] J. F. P. Gomes and C. G. Pinto, *Revista de Metalurgia*, 2006, vol. 42, pp. 409-16.

576 [10] D. J. Min, J. W. Han and W. S. Chung, Metall. *Mater. Trans. B*, 1999, vol. 30B,
577 pp. 215-21.

578 [11] B. Bhoi, A. K. Jouhari, H. S. Ray and V. N. Misra, *Ironmaking & Steelmaking*,
579 2006, vol. 33, pp. 245-52.

580 [12] A. Semykina, J. Nakano, S. Sridhar, V. Shatokha and S. Seetharaman, *Metall.*
581 *Mater. Trans. B*, 2010, vol. 41B, pp. 940-45.

582 [13] A. Semykina, *Metall. Mater. Trans. B*, 2012, vol. 43B, pp. 56-63.

583 [14] A. Semykina, J. Nakano, S. Sridhar, V. Shatokha and S. Seetharaman, *Metall.*
584 *Mater. Trans. B*, 2011, vol. 42B, pp. 471-76.

585 [15] D. Bhattacharjee, T. Mukharjee and V. Tathavadkar, "Set-up for production of
586 hydrogen gas by thermos-chemical decomposition of water using steel plant slag and
587 waste materials", Tata Steel Limited, Publication No.: WO2007125537 A1.

588 [16] T. Mukherjee and D. Bhattacharjee, "A Method for producing hydrogen and/or
589 other gases from steel plant wastes and waste heat", Tata Steel Limited, Publication
590 No.: WO2007036953 A1.

591 [17] H. Matsuura and F. Tsukihashi, *ISIJ Int.*, 2012, vol. 52, pp. 1503-12.

592 [18] M. Sato, H. Matsuura and F. Tsukihashi, *ISIJ Int.*, 2012, vol. 52, pp. 1500-1502.

593 [19] J. Li, D. Bhattacharjee, X. Hu, D. Zhang, S. Sridhar and Z. Li, *Mineral*
594 *Processing and Extractive Metallurgy*, 2017, vol. 126, pp. 94-105.

595 [20] J. Li, D. Bhattacharjee, X. Hu, D. Zhang, S. Sridhar and Z. Li, *Metall. Mater.*
596 *Trans. B*, 2019, vol. 50, pp. 1023-34.

597 [21] B.R. Sant and T.P. Prasad: *Talanta*, 1968, vol. 15, pp. 1483-86.

598 [22] K. L. Fetters and J. Chipman, *Trans. AIME*, 1941, vol. 145, pp. 95-112.

599 [23] E. T. Turkdogan and J. Pearson, *J. Iron Steel Inst.*, 1953. vol. 173, pp. 217-23.

600 [24] Z. Zhang, J. Li and P. Liu, *Journal of Iron and Steel Research International*,
601 2011, vol. 18, pp. 31-37.

602 [25] S. Esfahani, S. Mostaghel and M. Barati, *Journal of Non-Crystalline Solids*, 2016,
603 vol. 436, pp. 29-34.

604 [26] S. S. Jung and I. Sohn, Metall. *Mater. Trans. B*, 2012, vol. 43B, pp. 1530-39.

605 [27] M. Seo, C. Shi, J. Cho and S. Kim: *Metall. Mater. Trans. B*, 2014, vol. 45B, pp.

606 1874-86.

607 [28] X. Zhu, B. Ding, H. Wang, X. He, Y. Tan and Q. Liao: *Fuel*, 2018, vol. 219, pp.

608 132-40.

609 [29] H.Wang, B. Ding, X.Zhu, Y. Tan, X. He and Q. Liao: *International Journal of*

610 *Heat and Mass Transfer*, 2017, vol. 113, pp 286-94.

611 [30] J. Liu, G. Chen, P. Yan, B. Planpain, N. Moelans and M. Guo. *Journal of Crystal*

612 *Growth*, 2014, vol. 402, pp.1-8.

613 [31] K. Jackson: *Journal of Crystal Growth*, 2014, vol.264, pp. 174-86.

614 [32] J. Guo, M. Seo, C. Shi, J. Cho and S. Kim: *Metall. Mater. Trans. B*, 2016, vol. 47,

615 pp.2211-21.

616 [33] W. Xuan, K. J. Whitty, Q. Guan, D. Bi and J. Zhang, *Fuel*, 2014, vol. 137, pp.

617 193-99.

618 [34] D. Wang, M. Jiang, C. Liu, Y. Min, Y. Cui, J. Liu and Y. Zhang, *Steel Res.* Int.,

619 2012, vol. 83, pp. 189-96.

620 [35] S. Sridhar, K. C. Mills, O. D. C. Afrange, H. P. Lörz and R. Carli, *Ironmaking*

621 *& Steelmaking*, 2000, vol. 27, pp. 238-42.

622 [36] S. Esfahani and M. Barati, *Journal of Non-Crystalline Solids*, 2016, vol. 436, pp.

623 35-43.

624 [37] B. O. Mysen, L. W. Finger, D. Virgo and F. A. Seifert: *Am. Mineral*, 1982, vol.

625 67, pp. 686-95.

626 [38] S. Ueda, H. Koyo, T. Ikeda, Y. Kariya and M. Maeda: *ISIJ Int.*, 2000, vol. 40, pp.
627 739-43.
628 [39] S. Kashio, Y. Iguchi, T. Goto and Y. Nishina: *Trans. Iron Steel Inst. Jpn.*, 1980,
629 vol. 20, pp. 251-53.
630 [40] L. De Ferri, D. Bersani, A. Lorenzi, P.P. Lottici, G. Vezzalini and G. Simon: *J.*
631 *Non-Cryst. Solids*, 2012, vol. 358, pp. 814-19.
632 [41] L.D. Ferri, An. Lorenzi and P. P. Lottici: *Journal of Raman Spectroscopy*, 2016,
633 vol. 47, pp. 699-705.
634 [42] E.R. Lippincott, A. Vanvalkenburg, C.E. Weir and E.N. Bunting: *J. Res. Natl.*
635 *Bur. Stand.*, 1958, vol. 61, pp. 61-70.
636 [43] G. Matrajt, J. Borg, P.I. Raynal, Z. Djouadi, L. d'Hendecourt, G. Flynn and D.
637 Deboffle: *Astronomy and Astrophysics*, 2004, vol. 416, pp. 983-90.
638 [44] M.A. Karakassides, D. Gournis and D. Petridis: *Clay Minerals*, 1999, vol. 34, pp.
639 429-38.
640 [45] H.J. Stein: *Appl. Phys. Lett.*, 1986, vol. 48, pp. 1540-41.
641 [46] L.E. Russel: J. Soc. Glass Technol., 1957, vol. 41, pp. 304T.
642 [47] C. Orrling and A.W. Cramb: *Metall Mater Trans B*, 2000, vol. 31B, pp. 403-406.
643 [48] B.J.-Y. Baek, J.-W. Cho, and S.-H. Ki: *Metall Mater Trans B*, 2016, vol. 47B, pp.
644 32-36.
645 [49] L. J. Beyers, G. A. Brooks, B. Blanpain, and F. Verhaeghe: Proceedings of the
646 10^{th} International Conference on Molten Slags, Fluxes and Salts (MOLTEN16). TMS,
647 2016.

[50] K. C. Mills: The influence of structure on the physico-chemical properties of slags. *ISIJ International*, 1993, vol. 33 (1), pp. 148-155.

[51] X. Wu, X. Dong, R. Wang, H. Lv, F. Cao and X. Shen, *Journal of residuals science and technology*, 2016, vol. 13, pp. 57- 62.

[52] B. Lin, H. Wang, X. Zhu, Q. Liao and B. Ding: *Applied Thermal Engineering*, 2016, vol. 96, pp. 432-40.

[53] J. Li, Z. Guo, J. Gao and J. Li, *Metall Mater Trans B*, 2014, vol. 45B, pp. 1171-74.

[54] J. Li and Z. Guo, *Metall Mater Trans B*, 2014, vol. 45B, pp. 1272-80.

[55] J. Li, Z. Guo and J. Gao, *Ironmak Steelmak*, 2014, vol. 41, pp. 710-14.

[56] B. O. Mysen, L. W. Finger, D. Virgo and F. A. Seifert: *Am. Mineral*, 1982, vol. 67, pp. 686-95.

[57] S. Ueda, H. Koyo, T. Ikeda, Y. Kariya and M. Maeda: *ISIJ Int.*, 2000, vol. 40, pp. 739-43.

[58] S. Kashio, Y. Iguchi, T. Goto and Y. Nishina: *Trans. Iron Steel Inst. Jpn.*, 1980, vol. 20, pp. 251-53.

[59] K. Seo, M. Kim, S. Seok and D. H. Kim, *Colloids and Surfaces A: Physicochemical and Engineering Aspects*, 2016, vol. 492, pp 110-18.

[60] K. Malecha, *Sensors and Actuators B: Chemical*, 2013, vol. 181, pp 486-93.

[61] H. M. Khater, *International Journal of Civil and Structure Engineering*, 2012, vol. 2, pp 749-62.

[62] A. Ben Othman, F.Ayari, S. Mezguich and M. Trabelsi-Ayadi, *International Journal of Engineering Research & Technology*, 2016, vol. 5, pp 715-20.

[63] A. Kumar, D. Majumdar , S. Singhal , S. Agarwal , R. P. Badoni , K. M. Reddy,

Int. J. Pharm. Sci. Rev. Res., 2016, vol. 40, pp 6-11.

[64] X. Li, P. Jiang, Z. Wang and Y. Huang, Catalysts, 2016, vol. 6, pp 1-13.

[65] L. Skuja, K. Kajihara, J. Grube and H. Hosono, *AIP Conf. Proc.*, 2014, vol. 1624, pp 130-34.

[66] N. Boukhalfa and M. Boutahala, *Adsorption Science & Technology*, 2017, vol. 35, pp 20–36.

Table captions:

Table 1 Chemical Composition of Designed Slags and Pre-melted Slags Analyzed by XRF (Wt.%)

Table 2 Critical Cooling Rates of Slags with Different Basicities

Table 3 Peak parameters of the peaks of Raman spectra

Table 4 Distribution of the Q species

Table 5 EDS Analysis of Different Phase Areas in the Reacted Slag with Basicity of 1.0 at the Continuous Cooling Rate of 10 K/min, Corresponding to Figure 15(b) (Atomic Pct)

Table 6 Weight Fraction (%) of Crystallized Phases in the Un-reacted and Reacted Slags at the Continuous Cooling Rate of 10 K/min

Table 1 Chemical Composition of Designed Slags and Pre-melted Slags Analyzed by XRF (Wt.%)

	Slag 1		Slag 2		Slag 3	
	Designed	Measured	Designed	Measured	Designed	Measured
CaO	33.33	32.77	37.03	36.09	40.00	38.73
SiO_2	33.33	34.01	29.63	30.21	26.67	27.50
FeO	27.78	28.55	27.78	28.88	27.78	28.77
MnO	5.56	4.67	5.56	4.82	5.56	4.99
CaO/SiO_2	1.00	0.96	1.25	1.19	1.50	1.41

737 Table 2 Critical Cooling Rates of Slags with Different Basicities

	Basicity	$T_{\max}$ [K (°C)]	T_{nose} [K (°C)]	t_{nose} (S)	$R_{c,TTT}$ (K/min)
Slag1-U	1.00	1873 (1600)	1373 (1100)	77	390
Slag2-U	1.25	1873 (1600)	1523 (1250)	25	840
Slag3-U	1.50	1873 (1600)	1798 (1525)	3	1500
Slag1-R	1.00	1873 (1600)	1473 (1200)	89	269
Slag2-R	1.25	1873 (1600)	1523 (1250)	4	5250
Slag3-R	1.50	1873 (1600)	1698 (1425)	8	1313

U indicates the un-reacted slags, R indicates the reacted slags.

738

739

740

741

742

743

744

745

746

747

748

749

750

751

752 Table 3 Peak parameters of the peaks of Raman spectra

Species	Position (cm^{-1})	Area (%)	Refs.
Slag1-U			
Q^0	869	25.41	[37,38,39]
Q^1	919	28.97	[37,38,39]
Q^2	968	36.88	[37,38,39]
stretching of Si-O	1041	8.75	[40]
Slag1-R			
Asymmetric stretching of Si–O–Si	840	3.12	[41]
Q^0	861	16.71	[37,38,39]
Q^1	914	41.77	[37,38,39]
Q^2	966	0.65	[37,38,39]
Q^2	982	37.16	[37,38,39]
Q^3	1055	0.59	[37,38,39]
Slag2-U			
Q^0	859	1.41	[37,38,39]
Q^0	880	78.23	[37,38,39]
Q^1	912	10.40	[37,38,39]
Q^2	960	5.00	[37,38,39]
Q^3	1059	3.95	[37,38,39]
Asymmetric stretching of Si–O–Si	1163	1.01	[42]
Slag2-R			
Q^0	857	7.25	[37,38,39]
Q^0	880	62.86	[37,38,39]
Q^1	913	10.39	[37,38,39]
Q^2	963	16.65	[37,38,39]
Q^3	1100	2.84	[37,38,39]
Slag3-U			
Q^0	856	22.46	[37,38,39]
Q^0	880	66.04	[37,38,39]
Q^2	960	4.10	[37,38,39]
Stretching of Si-O	1017	6.76	[43]
Asymmetric stretching of Si–O–Si	1080	0.64	[44]
Slag3-R			
Q^0	856	53.94	[37,38,39]
Q^0	869	8.92	[37,38,39]
Stretching of Si-O	889	33.14	[45]
Q^2	978	2.55	[37,38,39]
Q^3	1099	1.45	[37,38,39]

753

754

755

Table 4 Distribution of the Q species

Slags	Q^0+Q^1	Q^2+Q^3	$(Q^0+Q^1)/(Q^2+Q^3)$
Slag1-U	54.38	36.88	1.47
Slag1-R	58.48	38.40	1.52
Slag2-U	90.04	8.95	10.06
Slag2-R	80.50	19.49	4.13
Slag3-U	88.50	4.10	21.59
Slag3-R	62.86	4.00	15.72

777 Table 5 EDS Analysis of Different Phase Areas in the Reacted Slag with Basicity of
778 1.0 at the Continuous Cooling Rate of 10 K/min, Corresponding to Figure 15(b)
779 (Atomic Pct)

	Ca	Si	Fe	Mn	O	SUM
P1	1.0	0.9	42.3	3.0	52.8	100
P2	1.0	1.0	42.1	2.9	52.9	100
P3	7.7	16.3	14.9	9.8	51.4	100
P4	9.0	15.3	13.5	9.2	52.9	100
P5	15.4	15.4	9.4	2.9	57.6	100
P6	15.4	15.7	9.7	3.0	56.1	100

780
781
782
783
784
785
786
787
788
789
790
791

792 Table 6 Weight Fraction (%) of Crystallized Phases in the Un-reacted and Reacted

793 Slags at the Continuous Cooling Rate of 10 K/min

Minerals	Slag1-U	Slag1-R	Slag2-R	Slag3-R
Magnetite (Fe_3O_4)	4	25	32	36
$CaFeSiO_4$	55	19	--	--
Ca_2SiO_4	--	--	35	37
$Ca(Mn, Ca)Si_2O_6$	41			
$CaMn_{0.32}Fe_{0.68}Si_2O_6$	--	51	--	--
$CaMn_{0.5}Fe_{0.5}O_{3-x}$	--	--	31	--
$Ca_2Mn_{0.34}Fe_{1.66}O_5$	--	--	--	26
Monoxide($(FeO)_x(MnO)_{1-x}$)	--	5	2	1

--: The amount of the phases is below the lower detection limit, U: un-reacted slags, R: reacted slags.

794

795

796

797

798

799

800

801

802

803

804

Figure captions

Figure 1 Thermal control of three different cooling processes.

Figure 2 Change in accumulated amount of different phases precipitated from slags with basicity of 1.00: (a) un-reacted slag and (b) reacted slag.

Figure 3 Change in accumulated amount of different phases precipitated from slags with basicity of 1.25: (a) un-reacted slag and (b) reacted slag.

Figure 4 Change in accumulated amount of different phases precipitated from slags with basicity of 1.50: (a) un-reacted slag and (b) reacted slag.

Figure 5 Crystallization process of reacted slag with basicity of 1.00 during isothermal region after quenching: (a)-(b) morphology of master slag at 473 K and at 1873 K, respectively; (c)-(i) crystallization process of reacted slag at the temperature of 1373 K for 729 S, 754 S, 829 S, 839 S, 849 S, 919 S, 934 S, respectively.

Figure 6 TTT diagram of un-reacted slags with different basicities.

Figure 7 TTT diagram of reacted slags with different basicities.

Figure 8 Crystallization process of un-reacted slag with basicity of 1.0 at the continuous cooling rate of 10 K/min: (a)-(b) morphology of master slag at 473 K and at 1873 K, respectively; (c)-(f) crystallization process of un-reacted slag at the temperature of 1331 K, 1330 K, 1329 K, 1328 K, respectively.

Figure 9 Crystallization process of reacted slag with basicity of 1.0 at the continuous cooling rate of 10 K/min: (a)-(b) morphology of master slag at 473 K and at 1873 K, respectively; (c)-(i) crystallization process of reacted slag at the temperature of 1482K, 1476 K, 1470 K, 1464 K, 1454 K, 1441 K, 1359 K, respectively.

827 Figure 10 CCT diagram for the un-reacted slags with different basicities (a) starting
828 crystallization of primary phase and (b) full crystallization of slag.
829 Figure 11 CCT diagram for the un-reacted slags with different basicities (a) starting
830 crystallization of primary phase and (b) full crystallization of slag.
831 Figure 12 Deconvoluted Raman spectra of amorphous slags with different basicities:
832 (a) Slag1-U; (b) Slag1-R; (c) Slag2-U; (d) Slag2-R; (e) Slag3-U; (f) Slag3-R.
833 Figure 13 Influence of cooling rate on undercooling degree of reacted slags with
834 different basicities.
835 Figure 14 Morphologies of the crystalline in the reacted slag with the basicity of 1.0 at
836 continuous cooling rate of 10 K/min (a) CLSM image and (b) SEM image.
837 Figure 15 SEM photographs of reacted slag with the basicity of 1.0 at the continuous
838 cooling rate of 10 K/min with different magnification factors: (a) 600X and (b)
839 1000X.
840 Figure 16 EDS map scanning of reacted slag with basicity of 1.0 at the continuous
841 cooling rate of 10 K/min.
842 Figure 17 X-ray diffraction patterns of reacted slag with the basicity of 1.00 at the
843 continuous cooling rate of 10 K/min.
844 Figure 18 X-ray diffraction patterns of reacted slag with the basicity of 1.25 at the
845 continuous cooling rate of 10 K/min.
846 Figure 19 X-ray diffraction patterns of reacted slag with the basicity of 1.50 at the
847 continuous cooling rate of 10 K/min.
848 Figure 20 X-ray diffraction patterns of un-reacted slag with the basicity of 1.00 at the

849 continuous cooling rate of 10 K/min.

850

851

852

853

854

855

856

857

858

859

860

861

862

863

864

865

866

867

868

869

870

Appendix

The structure of the amorphous slags (i.e. the quenched slags after reacting with moisture or holding in Ar gas) was analyzed by using a Perkin-Elmer 1600 Series FT-IR spectrometer. The FT-IR spectra were concentrated between 1200 and 800 cm^{-1} and deconvoluted by using Fityk 0.9.8 software, as shown in **Figure A1**. Accordingly, all the bands were assigned with the corresponding species and the relative abundance of each species semi-quantitatively expressed in their area percentage are listed in **Table A1.** From the results shown in **Figure A1** and **Table A1**, it can be seen that the symmetric stretching vibration of several types of band groups for Si corresponding to Q^0 (monomer), Q^1 (dimer), Q^2 (Chain) and Q^3 (sheet) was observed at about 850-880 cm^{-1}, 900-920 cm^{-1}, 950-980 cm^{-1} and 1050-1120 cm^{-1} respectively. The distribution of the Q species was examined and the values of $(Q^0+Q^1)/(Q^2+Q^3)$ were calculated to evaluate the depolymerization degree of the slags in **Table A2**. As shown in **Table A2**, with increasing the slag basicity from 1.0 to 1.5, the depolymerization degree, $(Q^0+Q^1)/(Q^2+Q^3)$, increases from 0.1 to 1.39 for the un-reacted slags and from 0.12 to 1.18 for the reacted slags. This is in agreement with the general belief that the basic oxide CaO, as a so-called network modifier, can depolymerize silicate network structure by the formation of non-bridging oxygen. As for the effect of gas atmosphere on the slag structure, the depolymerization degree for the un-reacted slags with basicity of 1.25 and 1.50 is higher than those for the reacted slags, while for the slags with basicity of 1.00, the depolymerization degree for the un-reacted slag is lower than that for the reacted slags. This trend agrees with the

results determined by Raman spectroscopy as shown in **Figure 12** in the main text.

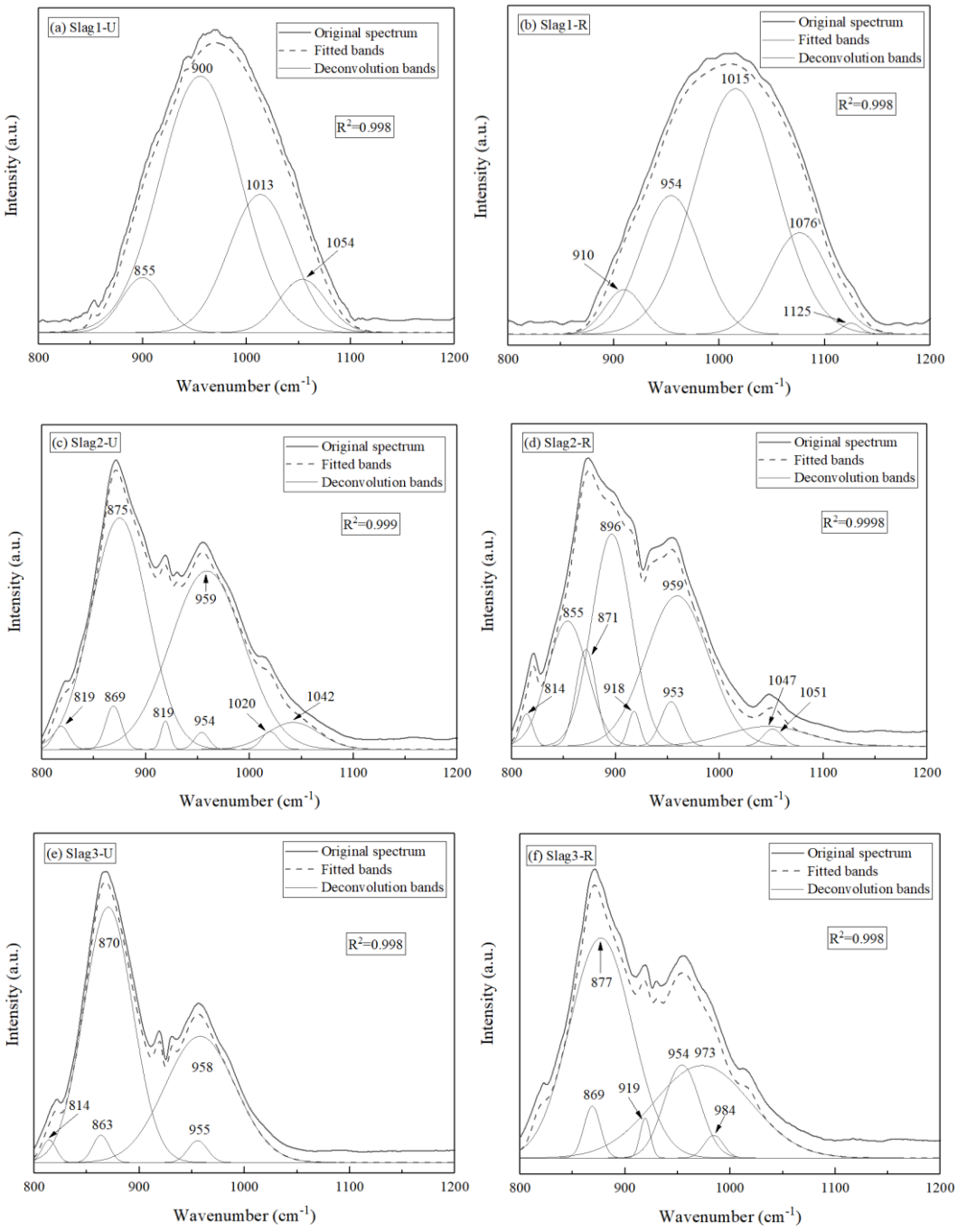

Figure A1 Deconvoluted FTIR transmittance of amorphous slags with different basicities: (a) Slag1-U; (b) Slag1-R; (c) Slag2-U; (d) Slag2-R; (e) Slag3-U; (f) Slag3-R

902 Table A1 Peak parameters of FTIR transmittance

Species	Position (cm^{-1})	Area (%)	Refs.
Slag1-U			
Q^1	900	6.77	[56,57,58]
Q^2	955	60.05	[56,57,58]
Stretching of Si-O-Si	1013	25.52	[59]
Q^3	1054	7.34	[56,57,58]
Slag1-R			
Q^1	910	3.12	[56,57,58]
Q^2	954	16.71	[56,57,58]
Asymmetric stretching of Si–O–Si	1015	41.77	[60]
Q^3	1076	0.65	[56,57,58]
Q^3	1125	37.16	[56,57,58]
Slag2-U			
Symmetric stretching of Si-O-Si	820	1.23	[61]
Q^0	869	2.34	[56,57,58]
Q^0	875	44.34	[56,57,58]
Q^1	919	1.00	[56,57,58]
Q^2	954	1.02	[56,57,58]
Q^2	959	44.13	[56,57,58]
Stretching of Si-O-Si	1020	1.07	[62]
Asymmetric stretching of Si-O-Si	1042	4.76	[63]
Slag2-R			
Symmetric and anti-symmetric stretching of Si–O–Si	814	1.38	[64]
Q^0	854	17.14	[56,57,58]
Stretching of Si-O	896	28.94	[65]
Q^2	953	3.12	[56,57,58]
Q^2	959	32.40	[56,57,58]
Stretching of Si-O	1047	5.59	[66]
Q^3	1051	1.12	[56,57,58]
Slag3-U			
Symmetric and anti-symmetric stretching of Si–O–Si	814	1.41	[64]
Q^0	864	1.97	[56,57,58]
Q^0	870	54.38	[56,57,58]
Q^2	955	1.87	[56,57,58]
Q^2	958	38.80	[56,57,58]
Slag3-R			
Q^0	869	3.03	[56,57,58]
Q^0	877	48.55	[56,57,58]
Q^1	919	1.43	[56,57,58]
Q^2	954	11.86	[56,57,58]

Q^2	973	31.50	[56,57,58]
Q^2	984	1.53	[56,57,58]

Table A2 Distribution of the Q species

Slags	Q^0+Q^1	Q^2+Q^3	$(Q^0+Q^1)/(Q^2+Q^3)$
Slag1-U	6.77	67.39	0.10
Slag1-R	4.64	39.72	0.12
Slag2-U	47.68	45.15	1.06
Slag2-R	25.11	36.64	0.68
Slag3-U	56.34	40.67	1.39
Slag3-R	53.01	44.89	1.18